Towards extended material probing using TLS and partial bidirectional reflectance distribution functions

Helena Laasch[1] (ORCID), Tomislav Medic[1] (ORCID) & Andreas Wieser[1] (ORCID)

[1] Institute of Geodesy and Photogrammetry, ETH Zürich, 8093 Zürich, Switzerland – (laaschh, tmedic, wiesera)@ethz.ch

DOI: 10.3217/978-3-99161-070-0-007, CC BY 4.0

Abstract

Terrestrial laser scanning (TLS) intensity values can provide meaningful information about scanned surfaces. Most reported TLS-based material probing attempts rely on deriving a reflectance constant per individual object surface, assuming that this reflectance primarily depends on the surface material properties. However, surface reflectance cannot be fully represented by a scalar value. Each surface exhibits complex reflectance patterns that can be represented by a characteristic bidirectional reflectance distribution function (BRDF), which encodes further material properties, surface roughness, and microstructure. While TLS data do not allow retrieval of the full BRDF, they do permit derivation of a special case thereof, corresponding to the configuration where illumination and observation directions coincide. We refer to this as the material-dependent angle-of-incidence compensation function (AOICOF).

We demonstrate that estimating the AOICOF from point clouds enables material identification. We achieve this by compensating the intensities for range dependence, segmenting the point clouds of a scene into surface patches, jointly processing patches with common material properties, and estimating AOICOF for each such group of surface patches. The AOICOFs estimated from the scans of the scene are then compared to a catalogue of reference functions obtained from laboratory measurements of various materials. We evaluate the agreement between in-situ and laboratory data by comparing their AOICOF and representative reflectance constants. Results demonstrate that obtained AOICOFs align closely with laboratory references, effectively allowing the distinction of material classes. While the shape of the AOICOF serves as a filter for narrowing down potential materials, we find that combining it with a representative reflectance constant helps distinguish between materials with similar AOI-dependent reflectance response. With these results, we demonstrate that reusing radiometric compensation functions enables extended material probing, providing a more comprehensive characterization of surfaces than a reflectance constant alone.

1 Introduction

Terrestrial laser scanning (TLS) is widely used in geodesy, surveying, and engineering applications to acquire dense and accurate 3D representations of real-world scenes. In addition to geometric information, TLS instruments record the intensity of the backscattered laser signal, which primarily depends on the scanner, the measurement configuration and the physical properties of the illuminated surface. As a result, TLS intensity has attracted interest as a source

of information for surface characterization, segmentation, and material-related analyses, such as moisture content estimation (Jin et al., 2021; Laasch et al., 2023) or roughness quantification (Lang, 2009).

To make TLS intensities independent of measurement configurations, numerous studies have focused on the radiometric compensation of distance and angle of incidence (AOI) effects (e.g., Kashani et al., 2015; Kaasalainen et al., 2011; Tan and Cheng, 2016; Jin et al., 2020; Laasch et al., 2025). In these approaches, the AOI dependence of the backscattered signal is explicitly modeled and compensated for, to subsequently retrieve a scalar that corresponds to the material-dependent reflectance at a predefined reference geometry – typically a fixed AOI (often perpendicular incidence). After this compensation, each point is assigned a single reflectance constant, which is then used for further processing or interpretation. This constant characterizes the material specifically at the scanner's operating wavelength. For ideal Lambertian surfaces, this single scalar is indeed sufficient to fully describe the reflectance behavior.

While this strategy has proved effective for improving radiometric consistency and enabling comparisons between scans taken at different locations, it implies that for non-Lambertian surfaces the AOI-dependent reflectance response itself is largely discarded once compensation is applied. From a physical perspective, however, AOI-dependent reflectance response is not merely a measurement artifact but reflects intrinsic surface properties. In optical remote sensing, AOI-dependent reflectance responses are commonly described by bidirectional reflectance distribution functions (BRDFs) that capture how reflectance varies with illumination and observation geometry. The BRDF is known to encode information about material composition, surface roughness, and microstructure (Cook and Torrance, 1982), and therefore, if such information can be retrieved, it can be used for extended material probing.

In TLS, the illumination and observation directions coincide due to the scanner's monostatic configuration. Consequently, the full BRDF cannot be observed. Instead, measurements are constrained to the backscattering direction, where the observation vector aligns with the illumination vector. By varying the incidence angle across the scene, TLS effectively samples a partial BRDF – specifically the intensity in the backscattering direction as a function of the AOI. This response is known to be strongly influenced by the surface material as well (Cook et al., 1982).

This material- and AOI-dependent reflectance response has been demonstrated in numerous studies. Laboratory experiments have shown that different materials exhibit distinct and reproducible AOI-dependent reflectance responses under controlled conditions (e.g., Kaasalainen et al., 2018). Similar AOI dependencies have also been observed in application-driven TLS studies, where AOI effects were estimated directly from field-acquired point clouds (in-situ) as part of radiometric compensation workflows (e.g., Li et al., 2023; Laasch et al., 2025). These studies consistently show that the AOI-dependent reflectance response reflects intrinsic surface characteristics.

In this paper, we build on these findings and investigate how material- and AOI-dependent reflectance responses can be exploited beyond radiometric compensation. Rather than treating the AOI effect solely as a systematic error to be removed, we investigate whether the material-dependent AOI compensation functions derived during radiometric calibration can serve as

informative descriptors for material identification. We interpret these functions as a partial BRDF corresponding to the backscattering configuration inherent to TLS and refer to them as AOI compensation functions (AOICOFs). Importantly, this interpretation does not replace established radiometric compensation workflows but extends them by reusing the estimated AOICOFs as material signatures.

This motivates the central question addressed in this paper: Given the challenges of in-situ data, is it feasible to use AOICOFs estimated from in-situ TLS point clouds for material identification? To answer this question, we estimate AOICOFs from real-world TLS scenes by first compensating intensities for range dependence, segmenting the point cloud into surface patches with similar material properties, and estimating the AOICOFs for each of those patches. We denote these field-estimated functions as in-situ AOICOFs. They are then compared to a catalogue of laboratory-derived reference AOICOFs for different materials. Similarity between functions is quantified, enabling a direct assessment of whether material-specific AOI-dependent reflectance responses can be recognized in the in-situ acquired TLS data and used for the enhanced material identification.

The remainder of this paper is structured as follows. Section 2 details the methods, including the description of the TLS datasets, the framework for estimating AOICOFs from point clouds, and the acquisition of independent laboratory reference measurements. It also defines the metrics used to evaluate both the AOICOF similarity and the reflectance constant similarity. Section 3 presents the results of the comparison between in-situ and laboratory data, analyzing the similarity of AOICOFs and of reflectance constants separately, and discusses the implications for material identification. Finally, Section 4 concludes the study and provides an outlook on the potential of AOICOFs for material identification.

2. Methods

2.1 In-situ acquired TLS dataset

This study uses the TLS datasets previously introduced in Laasch et al. (2025). The datasets were acquired using a Z+F Imager 5016 operating at a wavelength of 1550 nm. Prior to each acquisition, the scanner was warmed up for approximately one hour to reduce temperature-related intensity drift effects (Laasch et al., 2023). All data were collected in outdoor urban environments under stable meteorological and illumination conditions.

Two scenes were scanned (see Figure 1). Dataset 1 represents a contemporary urban environment comprising primarily plaster and wooden facades, complemented by vegetation, pavements, vehicles, and other urban elements. Dataset 2 corresponds to a historical urban setting dominated by a sandstone cathedral and surrounding streets, as well as vegetation and urban objects. Both scenes were acquired from a dense network of scan stations with an average inter-station spacing of approximately 5 m, resulting in a high degree of scan overlap. This dense acquisition geometry ensures that most surfaces were observed from multiple viewpoints and under a wide range of distances and AOIs. The datasets comprise approximately 30 scan stations per scene; detailed scan statistics are reported in Laasch et al. (2025).

For the present analysis, the datasets were manually segmented into homogeneous surface regions corresponding to individual materials. In Dataset 1, regions belonging to plaster and wooden facades were segmented. In Dataset 2, sandstone facades were segmented. Although these regions can be spatially disjoint, we group all points belonging to the same material into a single dataset for processing. In the remainder of this paper, we refer to this aggregated point set as a material segment.

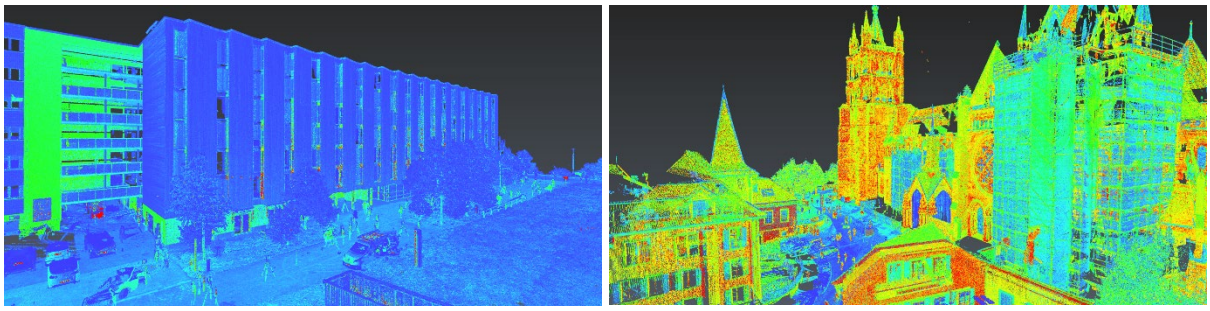

Fig. 1: Point clouds of the acquired datasets colored by raw intensity. Left: Dataset 1; Right: Dataset 2.

2.2 AOICOF estimation from in-situ point clouds

The estimation of AOICOFs follows an in-situ radiometric calibration framework, as described in Laasch et al. (2025). The key principle is to exploit the redundancy provided by overlapping TLS observations to estimate radiometric compensation functions directly from the acquired point clouds, without requiring dedicated laboratory measurements. The radiometric calibration is decomposed into a scanner-specific distance compensation function and a material-dependent AOICOF. The distance compensation function is assumed to be independent of material properties and is therefore estimated globally using the entire dataset. In contrast, the AOICOF is inherently material-dependent, as different surfaces exhibit distinct angular scattering behaviors. Consequently, AOICOFs are estimated separately, but simultaneously, for each material segment extracted from the point clouds (see Section 2.1).

Following the notation of Laasch et al. (2025), the raw recorded intensity values I_r are modeled as a product of a scanner constant κ_s, a material- and AOI-dependent term $f_{\varphi_0}^{mat}(\varphi)$, i.e., the AOICOF, a scanner- and distance-dependent term $g_{R_0}^{s}(R)$, and a material reflectance constant $\rho_{\varphi_0}^{mat}$:

$$I_r = \kappa_s \cdot f_{\varphi_0}^{mat}(\varphi) \cdot g_{R_0}^{s}(R) \cdot \rho_{\varphi_0}^{mat}, \tag{1}$$

where φ is the AOI, R is the distance, and φ_0 and R_0 are chosen reference AOI and distance. Due to the coupling between distance and AOI effects within the raw intensity data, Laasch et al. (2025) employed an iterative estimation scheme for radiometric calibration. It alternates between estimating the global range dependence $g_{R_0}^{s}(R)$ and all material-dependent, local, AOICOFs $f_{\varphi_0}^{mat}(\varphi)$ until convergence is reached. The AOICOF is normalized such that $f_{\varphi_0}^{mat}(\varphi_0) = 1$. In this work, we selected $\varphi_0 = 45°$, mitigating the influence of specular reflection and macroscopic surface roughness effects, which primarily affect reflectance at very low and very high AOIs, respectively.

To allow sufficient flexibility in modeling a wide range of angular reflectance behaviors, we employed smoothing splines to represent the AOICOFs $f_{\varphi_0}^{mat}(\varphi)$. This non-parametric approach avoids imposing a restrictive parametric form and enables the AOICOF to adapt to both diffuse and more complex angular scattering characteristics observed in real-world materials. As a result, a separate AOICOF is obtained for each manually predefined material segment, capturing its characteristic AOI-dependent reflectance response. By decoupling the range dependence and the AOI effects from the raw intensity, the method explicitly recovers the material reflectance constant scaled by the scanner constant (i.e., $\kappa_s \cdot \rho_{\varphi_0}^{mat}$).

2.3 Laboratory reference AOICOFs

To obtain a catalogue of independent reference AOICOFs, we conducted laboratory-based AOI experiments under controlled conditions with the same laser scanner (Z+F Imager 5016). We measured a total of five material types: sandstone, concrete, wood, plaster, and Spectralon. This selection comprises three materials that were also segmented within Datasets 1 and 2 to allow for direct comparison, and two non-matching materials that serve as controls. For each material, two distinct samples (small rectangular panels) were measured to capture intra-material variability. For the Spectralon, two panels with nominal reflectance values of 5% and 80% were used. All laboratory samples were externally sourced; they were chosen to be representative of the material types in the in-situ scenes (see Section 2.1), but were not physically extracted from the site.

Measurements were performed by systematically varying the AOI between the laser beam (line of sight) and the target surface (±85° in 1° steps) and recording raw intensities while keeping other acquisition parameters constant. To ensure that the derived functions were independent of distance effects, measurements were repeated at three different distances (12m, 20m, and 30m). For each sample, the recorded intensities captured at all three distances were first compensated for the known distance effect, combined, fitted with smoothing splines, and normalized so that $f_{\varphi_0}^{mat}(\varphi_0) = 1$ at $\varphi_0 = 45°$. This resulted in a separate laboratory reference AOICOF for each sample (5 materials × 2 samples). To establish a representative reference for each material type, these sample-specific functions were subsequently averaged (see Section 2.4).

2.4 AOICOFs similarity and reflectance constant similarity

To evaluate the correspondence between the in-situ and laboratory materials, we performed a similarity analysis based on the estimated AOICOFs and the reflectance constants.

AOICOF similarity

The similarity of the AOICOFs was assessed by comparing the AOICOFs $f_{\varphi_0}^{mat}(\varphi)$ derived from in-situ data with laboratory reference AOICOFs. All AOICOFs were discretized on a common AOI (φ) grid with a step size of 0.001 rad (arbitrarily chosen, dense to assure good function approximation). To obtain a representative reference for each material type (5 materials), we computed the mean of the two laboratory AOICOFs belonging to that class (1 material × 2 samples). The similarity between the in-situ AOICOF and the averaged laboratory

reference AOICOF was quantified using the root mean square error (RMSE) and the median absolute error (MAE), computed pointwise over the discretized AOI domain. The RMSE emphasizes larger deviations and is sensitive to localized mismatches, while the MAE provides a more robust measure of central deviation. Together, these metrics characterize the agreement of the AOICOFs, independent of absolute reflectance, as the functions are normalized to unity at the reference angle $\varphi_0 = 45°$.

Reflectance constant similarity

In addition to the shape-based similarity, we evaluated the similarity of the reflectance constants $\rho_{\varphi_0}^{mat}$. Since the system constant κ_s can be unknown, we cannot derive the reflectance $\rho_{\varphi_0}^{mat}$ directly. However, because all datasets (in-situ and laboratory) were acquired with the same scanner, κ_s is constant across all measurements. We therefore use the measurement configuration independent intensity I_{MCI}, which we introduced in Laasch et al. (2025). It represents the intensity compensated for distance and AOI effects:

$$I_{MCI} = \frac{I_r}{f_{\varphi_0}^{mat}(\varphi) \cdot g_{R_0}^{s}(R)} = \kappa_s \cdot \rho_{\varphi_0}^{mat} \tag{2}$$

The relative difference D_{rel} between the in-situ $I_{MCI}^{in-situ}$ and laboratory I_{MCI}^{lab} is calculated as:

$$D_{rel} = \frac{\left|I_{MCI}^{in-situ} - I_{MCI}^{lab}\right|}{(I_{MCI}^{in-situ} + I_{MCI}^{lab})/2} \tag{3}$$

In this ratio, the system constant κ_s cancels out, making D_{rel} a valid metric for comparing reflectance constants. Like for the AOICOF similarity analysis, we averaged the laboratory samples of the same materials for this metric.

3. Results

3.1 Shape-based similarity of AOICOFs

Figure 2 shows the AOICOFs derived from the in-situ TLS data (dashed) alongside the corresponding laboratory reference AOICOFs (solid) for three materials present in the in-situ TLS data. Visually, the in-situ AOICOFs exhibit a high degree of similarity to the laboratory-derived functions of the same material, indicating that the angular reflectance behavior estimated from in-situ point clouds is consistent with controlled laboratory measurements.

This observation is quantitatively supported by the AOICOF similarity metrics summarized in Table 1. For the plaster in-situ segment, the lowest RMSE and MAE values are obtained when it's AOICOF is compared to the laboratory plaster reference, allowing for a correct distinction form other materials. However, the difference to the 2nd most similar lab reference AOICOF (sandstone), is also small. The wood in-situ segment shows an even clearer distinction, with the

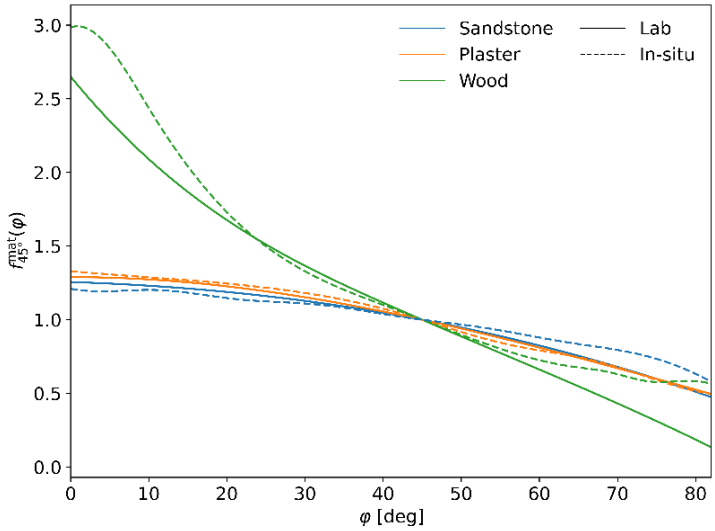

Fig. 2: AOICOFs - $f_{\varphi_0}^{mat}(\varphi)$, of three different materials estimated using the in-situ acquired TLS point clouds and their corresponding averaged lab AOICOFs.

smallest deviation regarding the laboratory wood reference, whereas comparisons to other materials result in substantially larger values of RMSE and MAE.

For the sandstone in-situ segment, material identification is more challenging. While the smallest deviation is observed for the Spectralon with 5% reference, the laboratory sandstone and plaster AOICOFs also exhibit low difference values. This indicates that multiple materials can exhibit very similar angular reflectance behavior, demonstrating that more information than just the AOICOF is needed to identify the material correctly.

Table 1: AOICOF similarity between the in-situ AOICOFs and averaged lab reference AOICOFs. The best metrics for each in-situ segment are highlighted in bold.

Lab\In-situ	**Plaster**		**Wood**		**Sandstone**	
	RSME	**MAE**	**RSME**	**MAE**	**RSME**	**MAE**
Sandstone	0.04	0.04	0.63	0.37	0.06	0.05
Concrete	0.17	0.10	0.47	0.29	0.24	0.18
Plaster	**0.02**	**0.02**	0.61	0.35	0.08	0.07
Wood	0.46	0.33	**0.22**	**0.16**	0.53	0.41
Spectralon 5%	0.11	0.10	0.67	0.43	**0.03**	**0.02**
Spectralon 80%	0.16	0.14	0.52	0.31	0.25	0.02

3.2 Reflectance similarity

In addition to AOICOF similarity, the reflectance constant similarity between in-situ segments and laboratory samples was evaluated as a second means for material separation. The similarity is computed using the relative difference (D_{rel}) of the I_{MCI} values (see Section 2.4). The results are summarized in Table 2.

Table 2: Reflectance similarity (D_{rel}) between in-situ segments and lab samples. The highest similarity (lowest difference) for each in-situ segment is highlighted in bold.

Lab\in-situ	Plaster	Wood	Sandstone
Sandstone	0.42	1.54	**0.00**
Concrete	0.65	1.43	0.24
Plaster	0.49	1.80	0.87
Wood	**0.01**	1.69	0.43
Spectralon 5%	1.50	**0.50**	1.28
Spectralon 80%	0.53	1.81	0.90

The reflectance-based comparison reveals substantial variability across material combinations. For several materials, large discrepancies between in-situ and lab reflectance values are observed, even when both belong to the same nominal material class. This is particularly evident for the wooden in-situ segment: the in-situ surface exhibits considerably lower reflectance than the laboratory wood samples. This arises simply because the specific varieties of material differ between the two settings: the wood in the in-situ scene is dark and glazed, whereas the laboratory samples are uncoated. A similar discrepancy in material composition is observed for the plaster.

In contrast, the sandstone material shows a close agreement between in-situ and lab reflectance values. We assume this is the case because the laboratory samples represent the same sandstone type found in-situ. Moreover, both the laboratory samples and the in-situ surfaces feature a raw, cut finish, ensuring similar surface properties. Consequently, for this material, the reflectance similarity resolves the ambiguity observed in the AOICOF similarity. For instance, while the sandstone AOICOF is very similar to Spectralon 5% and plaster, the reflectance comparison confirm the sandstone match and excludes the other two candidates.

As expected, these results indicate that reflectance similarity alone is not a reliable indicator for material identification, as it is a measure of absorption of the surface that is influenced by the material and the surface finishes (e.g., coating). Nevertheless, the reflectance constant carries undoubted value as a complementary metric, supplementing the AOICOF-based identification. Since both the reflectance constant and the AOICOF are derived simultaneously from the same data, they can be effectively integrated to support a more robust, multi-parameter material identification.

4. Conclusion

In this work, we investigated the potential of reusing radiometric calibration functions as physical descriptors for material probing and identification in terrestrial laser scanning (TLS). Standard radiometric compensation typically treats angular intensity variations as artifacts to be corrected. In contrast, we demonstrated that these variations encode intrinsic material properties that can be recovered from in-situ acquired point clouds. By estimating material-

dependent angle-of-incidence compensation functions (AOICOFs) – which approximate a partial bidirectional reflectance distribution function (BRDF) specific to the scanner's monostatic geometry – we showed that TLS data contains latent material information that supports material probing without requiring additional sensors.

Our experimental results confirm that in-situ AOICOFs derived from urban scenes align well with a catalogue of reference functions derived from controlled lab measurements, validating the approach for material identification. The analysis reveals that although the shape of the AOICOF serves as a strong feature for distinguishing materials, it is not unique; different materials with similar surface properties can exhibit similar AOICOFs. However, our results indicate that complementing the AOICOF similarity with reflectance similarity can improve material identification.

Despite the informational gain, neither the AOICOF nor the reflectance constant guarantees definitive identification in isolation. Different materials with similar surface properties can yield indistinguishable angular signatures, and materials with similar absorption can exhibit identical backscatter strengths. Therefore, the estimated AOICOFs serve to narrow down potential material candidates rather than providing a single, absolute classification. The effectiveness of combining these metrics depends on the complexity of the specific use case. While our study demonstrates the potential of this combination, determining the optimal mathematical framework to fuse angular shape and radiometric magnitude remains a subject for future work. Furthermore, in complex scenes with high material diversity, these geometric and radiometric cues should be supplemented with additional data sources as hyperspectral measurements (Han et al., 2023; Ray et al., 2024). Future research should investigate integrating AOICOFs with RGB color information, texture analysis, semantic scene context, or multi-spectral intensity data to resolve remaining ambiguities.

By shifting the perspective from removing angular effects to analyzing them, this work establishes a foundation for more semantically rich point cloud processing. It demonstrates that simultaneous geometric acquisition and physical surface characterization are feasible, offering a new dimension of information for remote sensing applications.

Acknowledgments

We thank Robert Presl for supporting the laboratory experiments. This work was supported by the ETH Research Grant “Protect Sandstone Monuments”.

Declaration of generative AI and AI-assisted technologies in the writing process

During the preparation of this work, the authors used ChatGPT and Gemini in order to improve readability and language. After using these tools, the authors reviewed and edited the content as needed and take full responsibility for the content of the publication.

Literature

COOK, R. L., & TORRANCE, K. E. (1982). A reflectance model for computer graphics. In: ACM Transactions on Graphics (ToG), 1(1), 7-24.

HAN, Y., SALIDO-MONZÚ, D., & WIESER, A. (2023). Classification of material and surface roughness using polarimetric multispectral LiDAR. In: Optical Engineering, 62(11), 114104-114104.

JIN, J., DE SLOOVER, L., VERBEURGT, J., STAL, C., DERUYTER, G., MONTREUIL, A.-L., DE MAEYER, P., & DE WULF, A. (2020). Measuring Surface Moisture on a Sandy Beach based on Corrected Intensity Data of a Mobile Terrestrial LiDAR. In: Remote Sensing, 12(2), 209.

JIN, J., VERBEURGT, J., DE SLOOVER, L., STAL, C., DERUYTER, G., MONTREUIL, A. L., VOS, S., DE MAEYER, P., & DE WULF, A. (2021). Monitoring spatiotemporal variation in beach surface moisture using a long-range terrestrial laser scanner. In: ISPRS Journal of Photogrammetry and Remote Sensing, 173, 195-208.

KAASALAINEN, S., JAAKKOLA, A., KAASALAINEN, M., KROOKS, A., & KUKKO, A. (2011). Analysis of incidence angle and distance effects on terrestrial laser scanner intensity: Search for correction methods. In: Remote sensing, 3(10), 2207-2221.

KAASALAINEN, S., ÅKERBLOM, M., NEVALAINEN, O., HAKALA, T., & KAASALAINEN, M. (2018). Uncertainty in multispectral lidar signals caused by incidence angle effects. In: Interface Focus, 8(2), 20170033.

KASHANI, A. G., OLSEN, M. J., PARRISH, C. E., & WILSON, N. (2015). A Review of LIDAR Radiometric Processing: From Ad Hoc Intensity Correction to Rigorous Radiometric Calibration. In: Sensors, 15(11), 28099-28128.

LAASCH, H., MEDIC, T., & WIESER, A. (2023). Towards Assessing Sandstone Surface Moisture and Degradation Level from Radiometrically Corrected TLS Intensity Data. In: ISPRS Annals of the Photogrammetry, Remote Sensing and Spatial Information Sciences, 10, 567-574.

LAASCH, H., MEDIC, T., PFEIFER, N., & WIESER, A. (2025). Automatic in-situ radiometric calibration of TLS: Compensating distance and angle of incidence effects using overlapping scans. In: ISPRS Journal of Photogrammetry and Remote Sensing, 228, 648-665.

LANG, M. W., & MCCARTY, G. W. (2009). Lidar intensity for improved detection of inundation below the forest canopy. In: Wetlands, 29(4), 1166-1178.

LI, X., SHANG, Y., HUA, B., YU, R., & HE, Y. (2023). LiDAR intensity correction for road marking detection. In: Optics and Lasers in Engineering, 160, 107240.

RAY, P., MEDIĆ, T., SALIDO-MONZÚ, D., & WIESER, A. (2024). High-precision hyperspectral laser scanning for improved radiometric correction of backscatter intensity. In: Optical Engineering, 63(5), 054110-054110.

TAN, K., & CHENG, X. (2016). Correction of incidence angle and distance effects on TLS intensity data based on reference targets. In: Remote Sensing, 8(3), 251.